

Article

Towards Investigating Surface Quality of Single-Crystal Silicon Optics Polished with Different Processes

Laixi Sun ^{1,†}, Yubin Zhang ^{1,2,†}, Xiaoyan Zhou ¹, Miaomiao Duan ¹ , Xin Ye ^{1,*}, Weihua Li ¹, Yaguo Li ³ and Liming Yang ^{1,3}

¹ Research Centre of Laser Fusion, China Academy of Engineering Physics, Mianyang 621900, China; sunlaixi@caep.cn (L.S.); zhangyubin21@gascaep.ac.cn (Y.Z.); zhouxiaoyan@caep.cn (X.Z.); duanmiaomiao19@gascaep.ac.cn (M.D.); liweihua@caep.cn (W.L.); yangliming@caep.cn (L.Y.)

² Joint Laboratory for Extreme Conditions Matter Properties, School of Science, Southwest University of Science and Technology, Mianyang 621010, China

³ Fine Optical Engineering Research Center, Chengdu 610041, China; yargolee@163.com

* Correspondence: yexin@caep.cn; Tel./Fax: +86-081-6248-0872

† These authors contributed equally to this work.

Abstract: A series of cleaning and etching experiments utilizing organic solvent or weak alkali solutions were performed on single-crystal silicon optics polished with different processes. Polishing-introduced fractured defects in the subsurface layer were systematically characterized using laser-induced scattering imaging and photothermal weak absorption imaging techniques. A white-light interferometer also measured the surface morphology and roughness of the samples to evaluate the surface quality of the optics. The results show that the organic solvent cleaning process can eliminate the surface contamination resulting from the environment and the near-surface polishing-introduced impurities but can not remove the fractured defects in the subsurface layer of the optics. By contrast, weak alkali solution can effectively expose the subsurface defects and decrease the concentration of the embedded absorbing impurities to some extent. The results also imply that the polishing process has a crucial effect on the surface quality (e.g., surface roughness and error) and optical performance (e.g., surface absorption) after the subsequent treatments such as cleaning or etching. The corresponding methodology of cleaning and characterization can serve as a predictive tool for evaluating the polishing level and laser damage resistance of the single-crystal silicon optics.

Keywords: silicon; SC images; weak absorption; defect detection



Citation: Sun, L.; Zhang, Y.; Zhou, X.; Duan, M.; Ye, X.; Li, W.; Li, Y.; Yang, L. Towards Investigating Surface Quality of Single-Crystal Silicon Optics Polished with Different Processes. *Coatings* **2022**, *12*, 158. <https://doi.org/10.3390/coatings12020158>

Academic Editor: Angela De Bonis

Received: 7 December 2021

Accepted: 21 January 2022

Published: 27 January 2022

Publisher's Note: MDPI stays neutral with regard to jurisdictional claims in published maps and institutional affiliations.



Copyright: © 2022 by the authors. Licensee MDPI, Basel, Switzerland. This article is an open access article distributed under the terms and conditions of the Creative Commons Attribution (CC BY) license (<https://creativecommons.org/licenses/by/4.0/>).

1. Introduction

Single-crystal silicon is an important semiconductor material with many applications in electronics, photovoltaics, and other disciplines. It is also an excellent infrared window material that is often used as a light filter, infrared window, and substrate material in various laser systems due to its high transmissivity in the mid-infrared band (3–5 μm) [1–5]. These applications generally require single-crystal silicon optics with high laser damage resistance and good surface quality associated with their polishing ability [6,7].

For decades, the study of laser-induced damage behavior of single-crystal silicon has attracted great interest. When silicon optics are irradiated by laser, the surface of the material absorbs the laser energy, leading to the rise in temperature. Irreversible material damage (e.g., cleavage fracture, melting, and evaporation) will occur when the laser fluence is increased to a certain level [8–12]. The typical damage morphology of the single-crystal silicon surface is shown in Figure 1. Figure 1 shows the scanning electron microscopy (SEM) imaging diagram of damage results of monocrystalline silicon optical element irradiated by a 3.8 μm Gaussian pulse laser (self-developed) for 60 s. The laser works in TEM00 mode with a frequency of 17 kHz. The laser pulse width is 25 ns, and the focal spot radius is 40 μm . The laser injection volume is 398 kW/cm^2 . Obvious ablation and resolidification

of the silicon material are observed. The damage crater is surrounded by a large number of solid particles of different sizes resulting from a considerable temperature gradient along the radial direction. The surface damage resistance degradation of single-crystal silicon is closely related to the existence of surface and subsurface defects produced during the fabrication process of the optics, as in many other optical materials such as fused silica [13–16]. Subsurface damage (SSD), which refers to residual fracture and deformed material (e.g., scratches and microcracks) produced by grinding and polishing operations, has been identified to be a primary damage precursor [17]. This is because surface fractures can serve as reservoirs for vanishingly small quantities of light-absorbing impurities. The type and concentration of the impurities are greatly influenced by the polishing process, such as abrasive powder type and diameter [18]. To date, how to minimize the presence of these damage precursors to fabricate high-quality single-crystal silicon optics is still a key challenge.

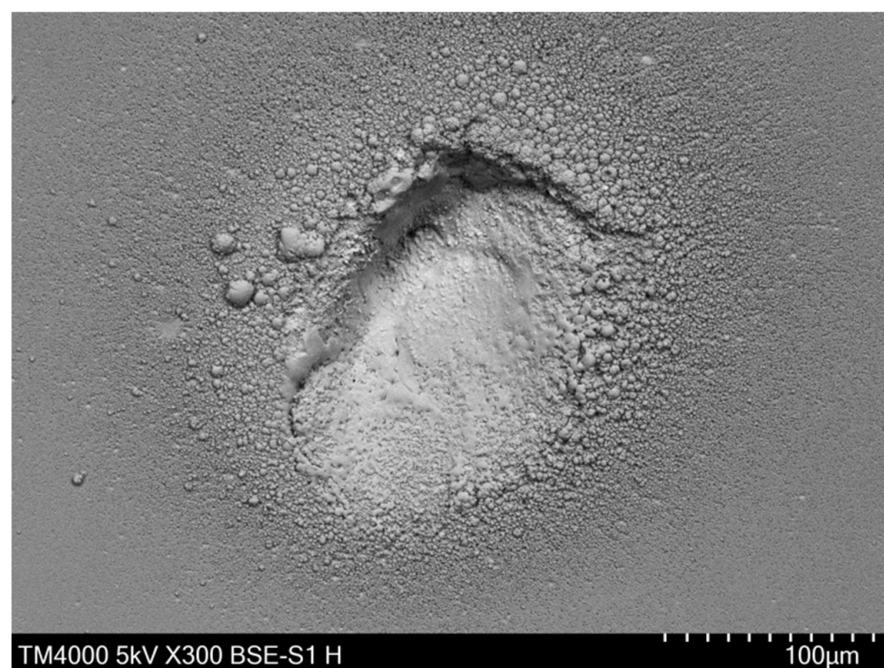


Figure 1. Typical damage morphology on single-crystal silicon surface observed by energy dispersive spectroscopy (EDS)-SEM. A 3.8 μm Gaussian pulse laser operating at TEM00 mode with a frequency of 17 kHz was used for the damage test. The pulse width and the focal spot radius were 25 ns and 40 μm , respectively. The damage was initiated at a laser intensity of 398 kW/cm^2 .

At present, based on the mature plasma dry chemical etching (DCE) and HF-wet etching technology, plasma-flexible modification of polished lenses can remove various surface and subsurface precursors without a trace. Silicon materials are more sensitive to the etching response of fluorine-containing plasma, and even the small change in plasma state may have a great influence on the physical and chemical characteristics of the monocrystalline silicon surface. In order to achieve flexible post-treatment, it is necessary to ensure that physical bombardment will not cause significant damage to the monocrystalline silicon surface, and the chemical reaction will not degrade the roughness and surface shape of the monocrystalline silicon surface. Therefore, it is necessary to study the influence of plasma generation conditions on the etching efficiency of the monocrystalline silicon surface.

The relationship between plasma distribution characteristics and surface quality characteristics such as surface roughness and surface shape of monocrystal silicon after etching was established through plasma diagnosis to minimize these damage precursors [19,20]. To improve the surface quality, it is necessary to detect and remove the polishing-induced SSD of the optics. Significantly, efficient detection of SSD can help improve the polishing

process and enhance the fabrication efficiency of single-crystal silicon optics. However, it is challenging to directly observe and detect the fractured defects hidden in the subsurface layer of the silicon optics through the naked eye or even conventional optical microscopy. For many years, both destructive and nondestructive methods have been developed for SSD detections [21]. For example, combined with traditional chemical wet etching, the SSD of silicon optics can be effectively displayed by laser-induced scattering (SC) imaging technology. SC imaging microscopy can detect the exposed physical structure features on the surface of transparent optical materials. Besides, photothermal weak absorption imaging spectroscopy, typically based on photothermal common-path interferometry (PCI), is another technique for SSD detection since absorption is a dominant characteristic for identifying the damage precursors. It utilizes the thermal lensing effect to nondestructively obtain the weak absorption characteristics of the near-surface region of the silicon materials [21–23].

The polishing of optical components is commonly divided into three kinds. The traditional polishing method belongs to the cold working method of glass. The polishing machine uses a friction wheel to rotate, the spindle speed is low, the plane swing tripod is used to apply pressure, and the pressure is adjusted by the load weight. The main advantages are that the precision requirements of the polishing machine are low, the replacement rate of the polishing mold is high, and the equipment investment cost is negligible. The main disadvantage is the low production efficiency. The chemical mechanical polishing method is a polishing method that combines chemical operation and mechanical action. First, the workpiece surface material reacts chemically with the oxidant and catalyst in the polishing liquid to form a soft layer that is relatively easy to remove. The process mainly removes the roughness of the surface to reach the average number of microns of tens of microns of finish. It is exposed again, and then the chemical reaction is carried out so that the surface polishing of the workpiece is completed in the alternating process of chemical and mechanical action. This avoids the surface damage caused by simple mechanical polishing and the disadvantages of slow polishing speed, poor surface flatness, and polishing consistency easily caused by simple chemical polishing. The magnetorheological polishing method is a flexible "small grinding head" with viscoplastic behavior formed by the rheology of the magnetorheological polishing liquid in a gradient magnetic field, and the workpiece has a rapid relative motion so that the surface of the workpiece is greatly affected. Shearing force ensures that the workpiece surface material is removed. The method is suitable for polishing optical parts of any geometric shape, with high processing speed, high efficiency, and high processing precision, with the processed surface roughness reaching nanometer level [24–27].

In the process of grinding and polishing optical components, a large number of defects and other precursors may be generated in the subsurface defect layer. The detection methods of these damage precursors, the relationship between them and the damage, and how to suppress it lacks relevant technical information. On the other hand, due to the lack of effective damage precursor characterization methods, there is relatively little research on the correlation between damage precursor and damage in high-energy laser systems. Therefore, it is of great significance to develop a comprehensive damage precursor detection system for different damage precursor types [21–27]. The main objective of this study is to investigate the surface quality of single-crystal silicon optics fabricated with different polishing processes through laser-induced SC imaging and photothermal weak absorption imaging techniques [28]. Two cleaning processes were chosen to provide different surface defect characteristics of the optics. During the experiments, we also utilized time of flight secondary ion mass spectroscopy (ToF-SIMS) and white-light interferometer to characterize the surface impurities and roughness of the optics [29]. Sample preparation and cleaning treatment are described in Section 2. The characterization and measurement results and the corresponding discussion are present in Section 3. We finally give the conclusion of the study in Section 4.

2. Experimental

In this study, we chose six different vendors to fabricate the single-crystal silicon optics (named vendors A, B, C, D, E, and F). All the silicon samples (orientation: 100) were 50 mm in diameter and 5 mm in thickness. The polishing processes the vendors used are shown in Table 1.

Table 1. Polishing details for the six vendors.

Sample	Polishing Process
A	Traditional polishing
B	Chemical mechanical polishing
C	Chemical mechanical polishing
D	Chemical mechanical polishing
E	Traditional polishing
F	Magnetorheological finishing

We utilized two chemical cleaning processes to treat the as-polished surface of the single-crystal silicon samples. One is an organic solvent (acetone and isopropyl alcohol, electronic grade, Kemiou Chemicals, Tianjin, Hebei, China) cleaning process that is used for eliminating the dust, oil, and a small number of impurities on the near-surface region of the optics. Another one is a weak alkali (Micro 90, major ingredient is ammonia, Burlington, NJ, USA) cleaning process, which can be used to slightly reveal the SSD and remove the embedded impurities. During the organic solvent cleaning process, the samples were first submerged in acetone solution for ultrasonic cleaning (45 °C for 10 min). Subsequently, the samples were removed and submerged in an isopropyl alcohol solution for ultrasonic cleaning (45 °C for 10 min). At last, the samples were removed and submerged in deionized water for ultrasonic rinsing (45 °C for 10 min). During the weak alkali cleaning process, the samples were first submerged in Micro 90 solution for ultrasonic cleaning (45 °C for 20 min) and then submerged in deionized water for ultrasonic rinsing (45 °C for 10 min). During the two cleaning processes, each silicon sample was constantly fixed by a Teflon clamp with the sample edge hold. The cleaning procedures were conducted in a seven-frequency ultrasonic cleaning machine at 40, 80, 120, 140, 170, 220, and 270 kHz. After the cleaning, the samples were spray rinsed using deionized water and allowed to air dry. The cleaning and drying processes were both implemented in the Class 100 cleanroom. The primary purpose of cleaning is to remove impurities on the surface of the silicon wafer (such as some organic matter, inorganic salts, metal, Si, SiO₂ dust). Monocrystalline silicon weak base (Micro 90) cleaning method is mainly through a chemical reaction to achieve anisotropic etching to if the monocrystalline silicon subsurface impurities, the etching rate is about 55 nm/h.

To perform this study, we utilized a self-developed laser-induced SC microscopy system that employed high-resolution imaging and high-sensitivity detecting techniques. We used a 532 nm laser source to excite the light-scattering feature (dark field) of the structural defects such as scratches, microcracks, and pits on the surface of the silicon samples. The SC signal was recorded with an electron multiplying charge-coupled device (EMCCD) detector (Edmund Optics Inc., Barrington, NJ, USA) with a spatial resolution of about 3.9 μm.

A photothermal weak absorption imaging system based on the PCI technique was used to investigate the absorbing defects on the sample surfaces [30,31]. One W quasi-continuous wave laser (3.8 μm) was used as a pump beam, and 5 mW He-Ne laser (632.8 nm) was used as a probe beam. The detection sensitivity of the system can approach 0.4 ppm. Before the measurement, the setup was first calibrated using a commercial metal-coated fused silica at 355 nm. A scanning strategy was executed across the sample surface to obtain two-dimensional absorption distribution (5 mm × 5 mm with the detecting step of 100 μm).

3. Results and Discussion

3.1. Samples after Organic Solvent Cleaning

Laser-induced SC imaging can be used as a tool for nondestructively detecting the surface characteristics of optical materials. This is an integrated microscope system consisting of a fluorescence microscope, a laser light source, a scan head that directs the laser light onto the sample and collects the emission, and a computer with software to control the scan head and display the acquisition. The system allows simultaneous measurement of fluorescence images and brightfield images. The excitation laser output power is about 50 mW, and the wavelength is 375 nm [32]. Figure 2 shows the typical SC feature of the sample surfaces fabricated with three different polished processes (Vendors A, B, and F). Note that many point features were visible on each cleaned sample surface, no matter which polishing process was chosen. We used Image-Pro software to obtain the size of each SC object by calculating the pixels they contained. Then it can be found that single-crystal silicon surfaces cleaned using the organic solvent process (acetone and isopropyl alcohol) mainly presented low-scale defects. These point defects were probably attributed to the presence of impurities in the polishing redeposition layer of the samples. An interesting phenomenon observed from the SC images was that the distribution (or density) of the point defects on each sample surface was very different. Compared with the sample polished by vendors A, the sample polished by vendor B had a relatively low density of the point defects (see the left and middle column of the images). Besides, an apparent nonuniform distribution of the point defects was observed on the surface of the sample polished by vendor F (see the right column of the images). The results indicated that, although it is not the subsurface characteristics, the SC features obtained by laser-induced SC imaging could initially exhibit the polishing quality of single-crystal silicon optics.

To recognize the characteristics of the point defects on the observed sample surfaces, we further extracted the total size (sum of the pixels) and the total count of the SC objects, as shown in Table 2. Through comparative analysis, several important pieces of information can be obtained. First, the sample polished by vendor F had the highest density (~19,400) of the point defects. Second, there was nearly the same total count of point defects on the sample surfaces polished by vendors A and F. Third, the sample polished by vendor B had the smallest total size (~8393) and total count (~83) of the point defects. The results indicated that the surface quality of the single-crystal silicon optics was greatly dependent on the polishing process. The laser-induced SC imaging technique can be utilized as a tool to nondestructively detect the polishing-induced impurities on the single-crystal silicon surface.

Table 2. Detailed information of the detected SC signals on the sample surfaces: total size (sum of the pixels) and total count of the point defects.

	Total Size	Total Count
Vendor A	13,546	193
Vendor B	8393	83
Vendor F	19,400	202

ToF-SIMS was conducted to characterize the type and relative concentration of the impurities in the polishing redeposition layer of the samples polished by vendors D and F, as shown in Figure 3. During the measurement, a Bi⁺ ion beam with the energy of 30 keV was used as the initial ion source, while a O²⁺ ion beam with the energy of 1 keV was used as the sputtering ion source. The sputtering angle of the ion beam was 45°. The scanning area was 200 µm × 200 µm. The detecting position on each sample surface was randomly selected. The detected elements mainly contained B, Na, Mg, Al, K, Ca, Fe, and Cr. The intensity of the detected ions has been normalized with silicon particle number (counts 10,000) as a standard. It can be noted from Figure 3 that there were a significant number of impurities on the polished sample surfaces. The peak concentrations of these

impurity elements were all located on the surface and dropped sharply with the increase of the detecting depth. It can also be noted that the concentration and embedding depth of the impurities in the sample surface was greatly influenced by the polishing process. The sample polished by vendors A, K, and Fe elements had a relatively high concentration on the silicon surface. Both impurities maintained a nearly steady level even when the detecting depth was up to about 60 nm. On the surface of the sample polished by vendor B, the Cr element had the highest concentration on the surface roughness of the sample (with a relative intensity of $\sim 10^5$). An apparent linear decline of the Cr concentration was observed with the increase of detecting depth. Except for the Cr element, the concentrations of all other elements dropped in exponential decay. The relative concentrations of the impurities gradually approached zero when the detecting depth increased to about 60 nm. For the vendor F polished sample, the results were quite different. First, not Cr, but Al was a dominant impurity element enriched on the sample surface. The maximal intensity of the Al element was only about $\sim 10^4$ (also dropped linear decay with detecting depth increased). Second, compared with the vendor A polished sample, the maximal intensity of Cr element on the vendor F polished sample surface decreased nearly two orders of magnitude (from $\sim 10^5$ to $\sim 10^3$). Third, the relative concentration of the impurities approached stabilization at about 30 nm detecting depth.

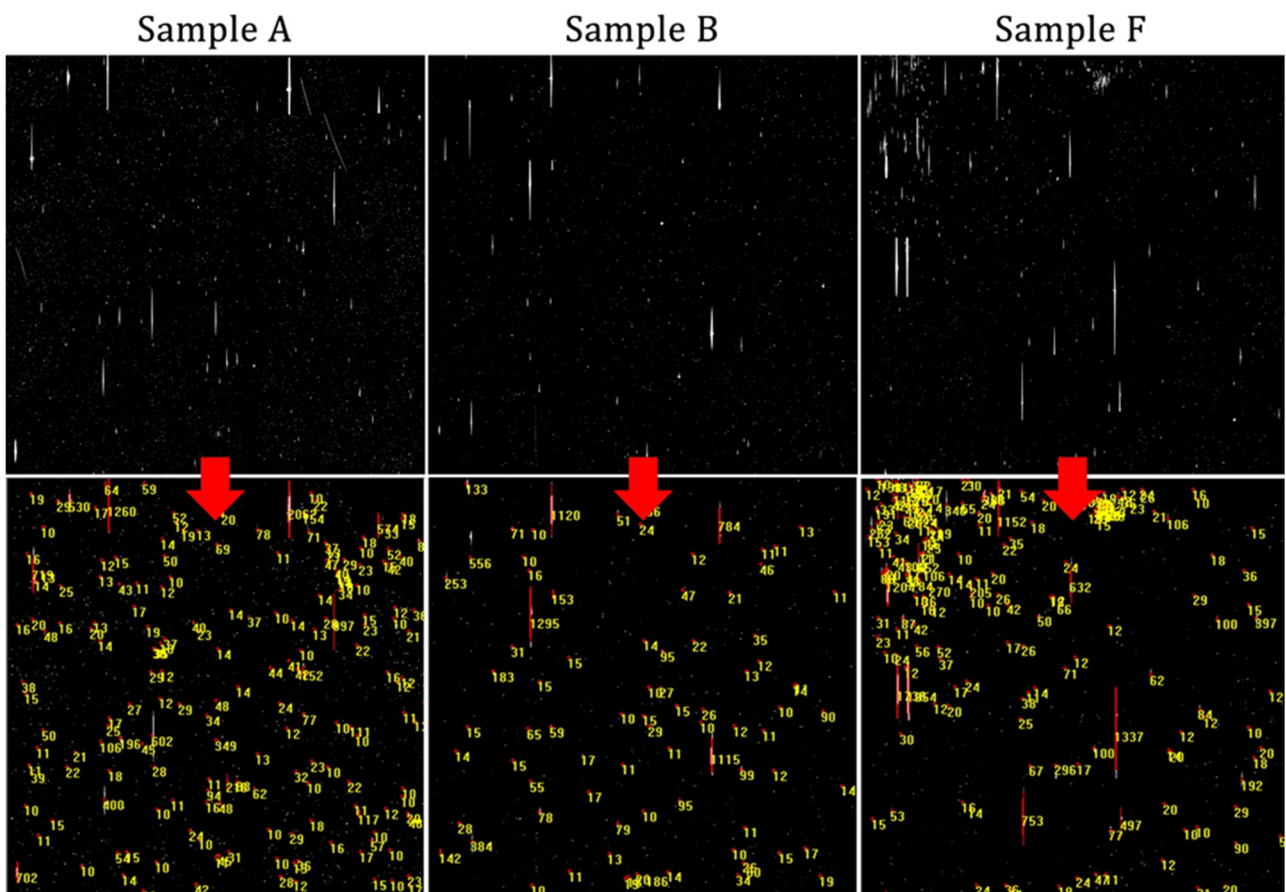


Figure 2. SC images of the sample surfaces fabricated with three different polishing processes (Vendors A, B, and F). The first row of images shows the initial results of the SC signals obtained by the SC imaging system. The second row shows the statistical results of the SC signals corresponding to the original results analyzed by the Image-Pro software. Yellow numbers on each image indicate the sizes (number of pixels) of SC objects. Only objects with a size larger than 10 pixels were marked. Each image measures 1.2 mm per side.

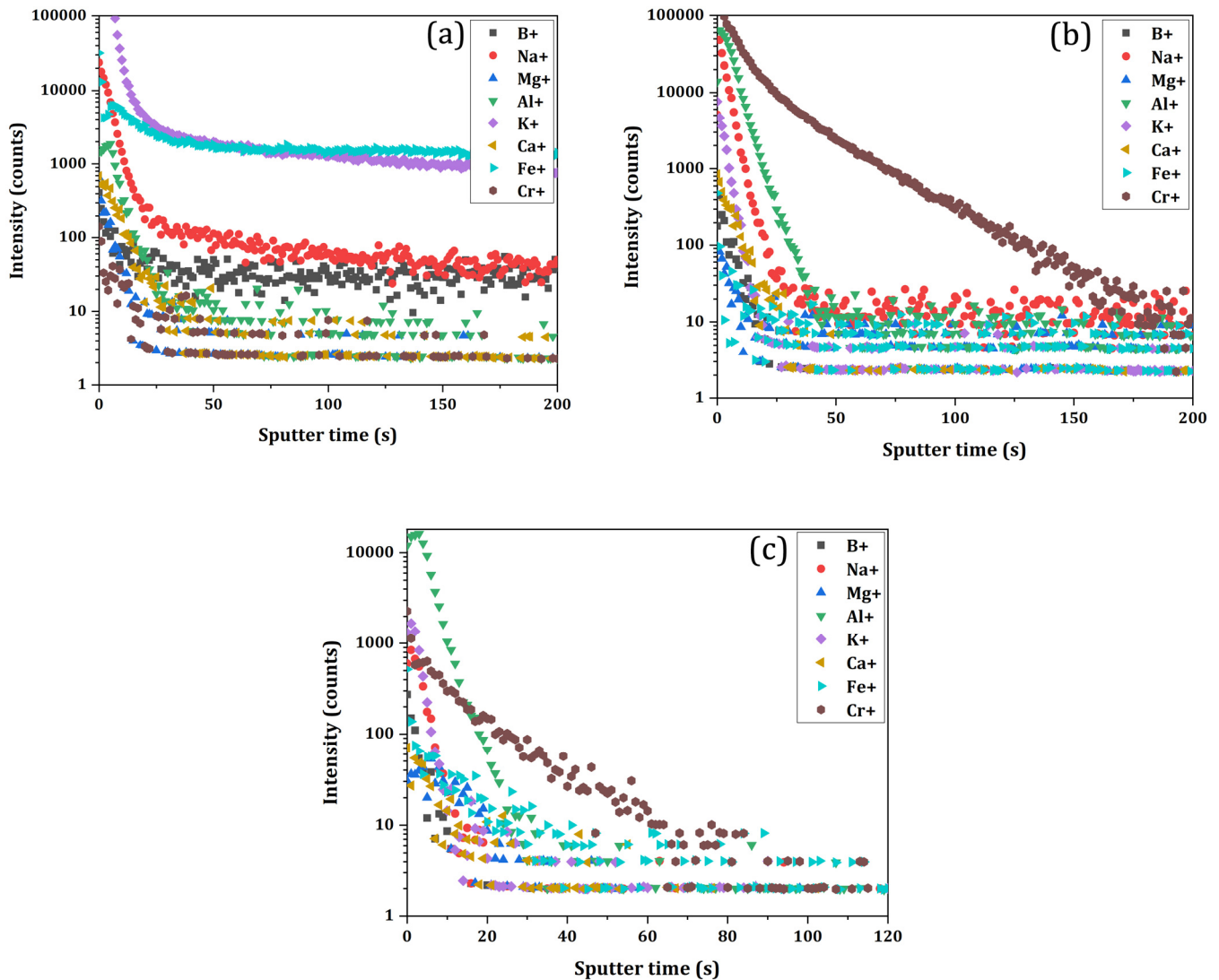


Figure 3. Depth profiles of impurities obtained from ToF-SIMS on the surfaces of the samples typically polished by (a) vendor A, (b) vendor B, and (c) vendor F. The sputter rate of the material was 0.33 nm/s.

The concentration and embedding depth of the impurities on the sample surface are mainly influenced by the polishing process of the optics. For example, Fe is the main absorbing element on silicon surface polished by vendor A. It is probably due to Fe-containing polishing power or implements during the traditional polishing process. Vendor B conducts the fabrication of the silicon optics using a chemical–mechanical polishing method, where a polishing head with a main component of Cr was used. Therefore, the Cr element will be enriched on the polished silicon surface. Differently, vendor F uses a magnetorheological finishing technique to fabricate the optical surface of the silicon, causing a significant amount of Al impurities to remain on the silicon surface. These variations in concentration and embedding depth of the impurities can affect the surface absorption level of the single-crystal silicon optics under laser irradiation. Optimization of the polishing process to minimize the damage precursors will be suitable for enhancing the damage threshold of the optics [33].

Photothermal weak absorption measurement was carried out on the three sample surfaces. The pump beam is a 355 nm quasi-continuous laser with 1 W output power and was focused on the sample surface with a 60 μm focal spot ($1/e^2$). The probe beam

is a modulated He-Ne laser that overlapped with the pump laser on the surface of tested samples. When an absorption defect appears on the surface of the optical material, the pump laser energy is partially absorbed and induces a change in the reflection index of the optical material, which will lead to the deflection of the optical axis of the probe laser. We can use a position sensor and a lock-in amplifier to extract the weak signal changes and then calculate the absorption coefficient of the material on the pump laser [32]. The absorption maps of the spatial scan in a square area of 20 mm \times 20 mm are shown in Figure 4. The mean and maximum absorption values are summarized in Table 2. It can be seen from the figure that there were a large number of discrete absorbing defects on all the sample surfaces. As shown in Table 3, the vendor A polished surface had a relatively low mean absorption level (2.77 ppm). For the samples polished by vendors B and F, their mean absorption levels were nearly the same (3.57 ppm and 3.68 ppm, respectively). Besides, it can be noted that the vendor F polished surface had some high-absorption defects, and the maximum absorption value was 46.58 ppm. The results indicated that the weak-absorption detecting technique could be used as a nondestructive method to evaluate the polishing level of single-crystal silicon optics. However, because the measured results are relatively macroscopic, it is difficult to identify the form or morphology of the defects.

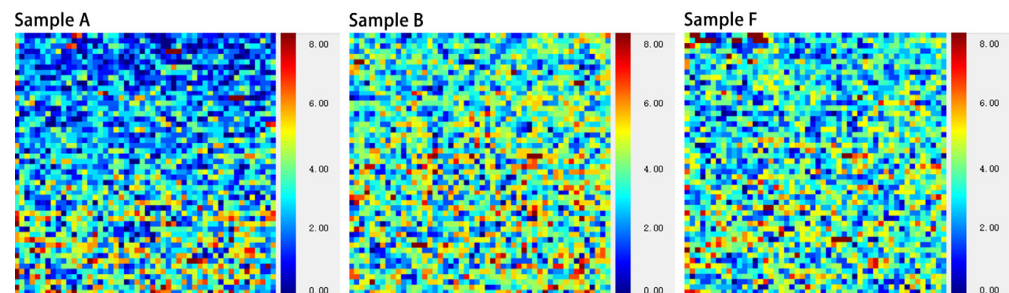


Figure 4. Weak absorption map of the sample surfaces polished by different vendors. The spatial scanning area was 20 mm \times 20 mm square.

Table 3. The mean and maximum absorption value of the measured area on the surface of the samples.

Vendor	Mean	Max
A	2.77	29.38
B	3.57	16.02
F	3.68	46.58

3.2. Samples after Weak Alkali Cleaning

We investigated the effect of the polishing process on the surface quality of the single-crystal silicon optics that have been cleaned by weak alkali solution. We first compared the SC imaging results of two typical samples (samples B and F) before and after the weak alkali cleaning, as shown in Figure 5. Many SC features were observed on the uncleaned sample surfaces, especially for the vendor B polished sample [see Figure 5a]. The discrete SC features were probably due to the polishing-introduced impurities and the environmental contamination. For the uncleaned samples, it can also be noted from Figure 5a,c that the surface treated by vendor B had slight scratches, while the surface treated by vendor F had no apparent scratches. When the two samples underwent weak alkali cleaning, we noticed that visible scratches existed on the sample surfaces [see Figure 5b,d]. It is because the weak alkali can slightly etch the optical surface of the single-crystal silicon and expose the subsurface defects introduced during the grinding or polishing processes. For the cleaned samples, an interesting phenomenon that can be observed is that vendor F polished surface had a much higher density and larger scale of the exposed scratches than vendor B polished surface. The results indicated that the initial quality of the grinding and polishing processes prior to the weak alkali cleaning is crucial for the surface quality (e.g., surface

roughness (R_q) and error) after the subsequent treatments such as cleaning or etching. The results also indicated that the organic solvent cleaning can considerably remove the surface contamination and near-surface impurities but can not effectively expose the fractured defects in the subsurface layer of the optics.

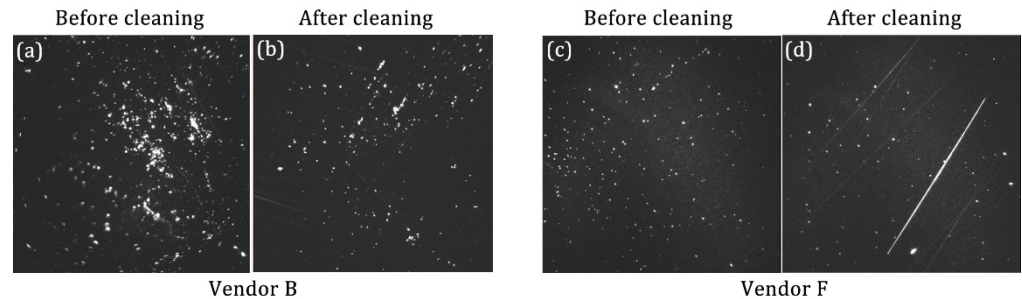


Figure 5. Two sets of light-scattering images both before and after the weak alkali cleaning on the surface of the samples polished by vendors B (a,b), and F (c,d). Each image measures 1.2 mm per side.

To deeply investigate the effect of the polishing process on the surface quality of the single-crystal silicon, we cleaned six silicon samples fabricated by different vendors using the weak alkali solution and then observed their corresponding SC images. As shown in Figure 6, it can be noted that the SC feature on the sample surface was dramatically dependent on the polishing process. Vendor A polished surface (see Figure 6a) showed the highest density and scale of scratches, which initially surprised us since the surface of this sample cleaned with organic solvent had no obvious scratches (see Figure 2). Except for vendor C, all other vendors greatly scratched the optical surfaces of the silicon samples during their polishing processes. However, the largest amount of point defects that featured light scattering were observed on the sample surface polished by vendor C. These point defects might be attributed to the exposed pits resulting from the detachment of the remaining particles during the polishing process. The comparison makes us believe that vendor B had the best polishing level since the least amount of SSD (scratches and pits) was observed on the sample surface. Hence, the combination of weak alkali cleaning and laser-induced SC imaging can be used to evaluate the polishing process of single-crystal silicon optics.

The white light interferometer was used to investigate the morphology and surface roughness (at submillimeter scale) of the samples polished by different vendors [34]. Figure 7 shows the microscope images of the sample surfaces with the detecting area of $180\ \mu\text{m} \times 250\ \mu\text{m}$. The corresponding measured surface roughness values are shown in Figure 8, reflecting the surface polishing quality of monocrystalline silicon optical elements. Consistent with the SC observation from Figure 6, the sample polished by vendor B had the lowest surface roughness (only 0.227 nm), indicating that the least amount of SSD was introduced during the polishing. As expected, other vendors polished optical surfaces had a relatively high roughness, especially for the sample polished by vendor A (0.602 nm). The 3D micrographs shown in Figure 7 give a deeper insight into how the polishing process affects the surface quality in terms of the SSD as well as the surface roughness of the sample after the SSD is exposed by weak alkali. For vendor A polished sample, large-scale scratches were observed on the surface. The width and depth of some scratches were extremely large, causing a dramatic increase in surface roughness. Although the scale of the exposed scratches on the surfaces polished by vendors D, E, and F was a little lower, these scratches had a relatively high density which still achieved the very rough surfaces (0.475, 0.523, and 0.468 nm, respectively). Another interesting phenomenon observed from Figure 7 was that vendor C produced no scratches but many island structures on the single-crystal silicon surface. These structures, which have also been exhibited by the SC imaging, give rise to the high surface roughness of the sample (0.474 nm).

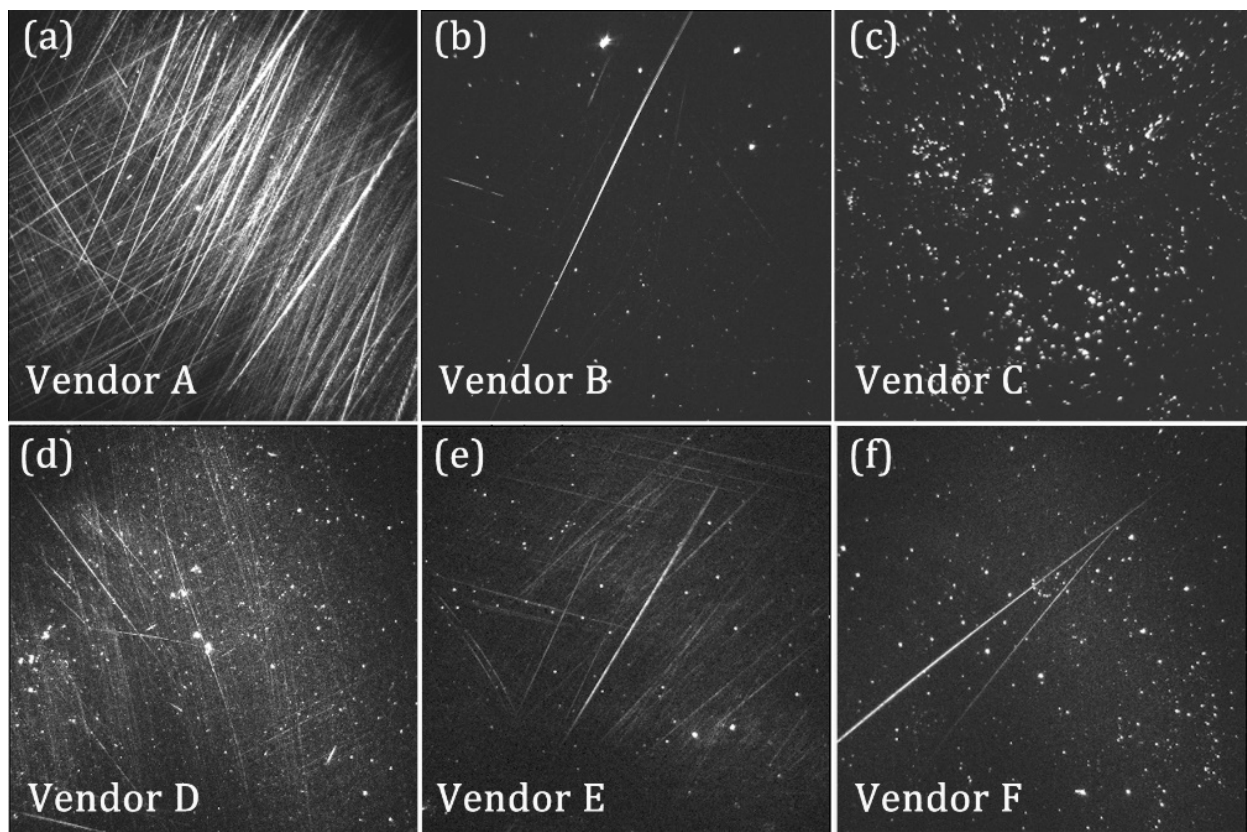


Figure 6. Light-scattering images after weak alkali cleaning of the samples polished by different vendors. Each image measures 1.2 mm per side. (a) Traditional polishing; (b) Chemical mechanical polishing; (c) Chemical mechanical polishing; (d) Chemical mechanical polishing; (e) Traditional polishing; (f) Magnetorheological finishing.

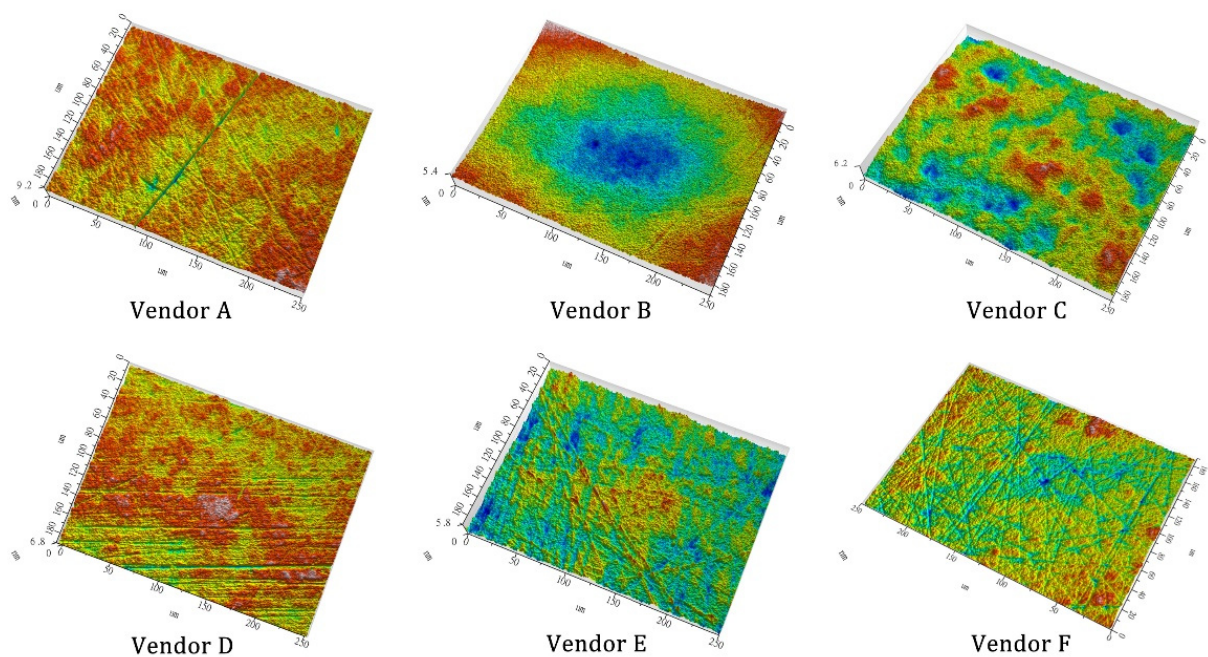


Figure 7. 3D micrographs of the sample surfaces polished by different vendors obtained through the white light interferometer.

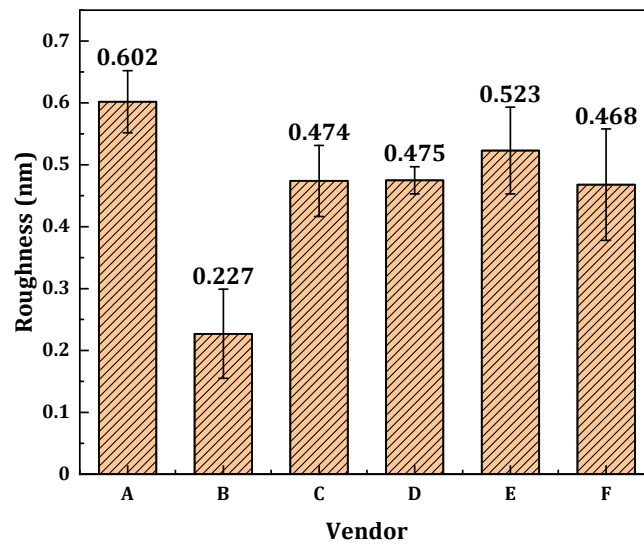


Figure 8. Roughness of the samples with different polishing processes (submillimeter scale).

Figure 9 shows the mean absorption level for all the silicon samples investigated in this study after cleaning with the weak alkali solution, reflecting the average absorption of impurities and defects in the subsurface of monocrystalline silicon optical elements. The scanning parameters were strictly the same as those used for the samples cleaned with an organic solvent. Note that the absorption levels of the samples were decreased after the weak alkali cleaning. This is probably due to the removal of the impurities in the near surfaces of the samples [35]. The sample surface polished by vendor B had a relatively low absorption level. However, the difference in mean absorption among these samples was not obvious. We believe that the absorption level of the sample after weak alkali cleaning is very dependent on the polishing process. For example, the deep SSD layer might not be effectively removed during the weak alkali cleaning process. The remaining defects will still absorb the laser light energy causing the increase of the mean absorption.

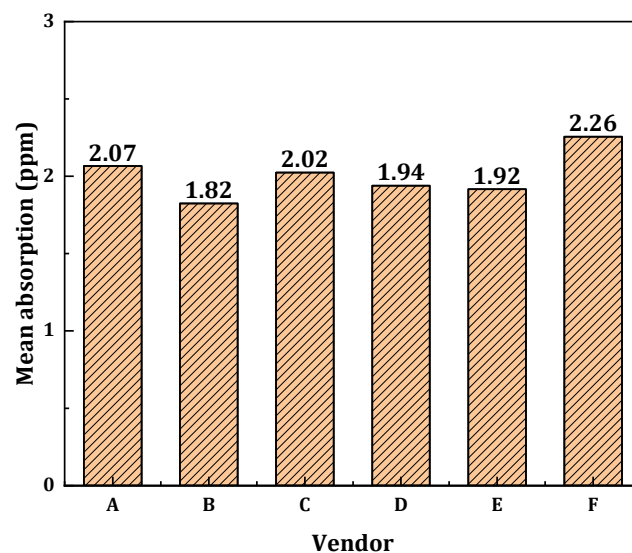


Figure 9. Mean absorption of the samples polished with different vendors. The spatial scanning area was also a 20 mm × 20 mm square.

4. Conclusions

Several single-crystal silicon optics with different polished processes have been treated with two chemical cleaning routes. Optics with different polishes may have a good finish

before the inspection. The organic solvent cleaning process (using acetone and isopropyl alcohol) can eliminate the surface contamination resulting from the environment and the near-surface polishing-induced impurities but cannot expose the fractured defects in the subsurface layer of the optics. Therefore, the high surface finish of the optical element does not mean that the surface of the optical element has fewer defects. Slight etching by weak alkali cleaning process resulting in the exposure of SSD has been achieved. The relative amount of SSD can be easily visually compared by using laser-induced SC imaging techniques. This methodology offers utility as a diagnostic to expose subsurface mechanical damage created during optical fabrication as well as a strategy to improve the laser-induced damage resistance of the optics.

Author Contributions: Conceptualization, formal analysis, investigation, data curation, writing—original draft, writing—review & editing, funding acquisition, L.S.; conceptualization, formal analysis, investigation, data curation, revision, Y.Z.; conceptualization, formal analysis, investigation, X.Z.; conceptualization, formal analysis, revision, M.D.; conceptualization, formal analysis, revision, X.Y.; conceptualization, formal analysis, revision, W.L.; formal analysis, funding acquisition, Y.L.; conceptualization, formal analysis, revision L.Y. All authors have read and agreed to the published version of the manuscript.

Funding: The authors are grateful for the support of the National Natural Science Foundation of China (NSFC) (62175222, 61705204, 61705206, 62005258, and 61805221). Laser Fusion Research Center Funds for Young Talents (RCFPD3-2019-2) and Foundation of Science and Technology on Plasma Physics Laboratory of China Academy of Engineering Physics (2018).

Institutional Review Board Statement: Not applicable.

Informed Consent Statement: Not applicable.

Acknowledgments: The authors wish to acknowledge the photothermal weak absorption measurement performed by Hao Cui and thank Eceshi for the ToF-SIMS analysis.

Conflicts of Interest: The authors declare no conflict of interest.

Declaration of Competing Interest: The authors declare that they have no known competing financial interests or personal relationships that could have appeared to influence the work reported in this paper.

References

1. Chen, Y.; Lu, J.; Ni, Z. Analysis of thermal stress damage in single-crystal silicon induced by 1064nm long pulse laser. *Proc. SPIE* **2007**, *6835*, 68351X.
2. Zeng, Y.; Chen, X.F.; Yi, Z.; Yi, Y.G.; Xu, X.B. Fabrication of p-n heterostructure ZnO/Si moth-eye structures: Antireflection, enhanced charge separation and photocatalytic properties. *Appl. Surf. Sci.* **2018**, *441*, 40–48. [[CrossRef](#)]
3. Deng, Y.; Cao, G.; Wu, Y.; Zhou, X.; Liao, W. Theoretical description of dynamic transmission characteristics in MDM waveguide aperture-side-coupled with ring cavity. *Plasmonics* **2015**, *10*, 1537–1543. [[CrossRef](#)]
4. Zhou, F.; Qin, F.; Yi, Z.; Yao, W.; Liu, Z.; Wu, X.; Wu, P. Ultra-wideband and wide-angle perfect solar energy absorber based on Ti nanorings surface plasmon resonance. *Phys. Chem. Chem. Phys.* **2021**, *23*, 17041–17048. [[CrossRef](#)]
5. Zhao, F.; Chen, X.; Yi, Z.; Qin, F.; Tang, Y.; Yao, W.; Yi, Y. Study on the solar energy absorption of hybrid solar cells with trapezoid-pyramidal structure based PEDOT:PSS/c-Ge. *Sol. Energy* **2020**, *204*, 635–643. [[CrossRef](#)]
6. Zhao, J.; Jiang, E.; Qi, H.; Ji, S.; Chen, Z. A novel polishing method for single-crystal silicon using the cavitation rotary abrasive flow. *Precis. Eng.* **2020**, *61*, 72–81. [[CrossRef](#)]
7. Chen, X.; Gu, Y.; Lin, J.; Yi, A.; Kang, M.; Cang, X. Study on subsurface damage and surface quality of silicon carbide ceramic induced by a novel non-resonant vibration-assisted roll-type polishing. *J. Mater. Process. Technol.* **2020**, *282*, 116667. [[CrossRef](#)]
8. Fu, C.J.; Zhang, Z.M. Nanoscale radiation heat transfer for silicon at different doping levels. *Int. J. Heat Mass Transf.* **2006**, *49*, 1703–1718. [[CrossRef](#)]
9. Deng, Y.; Cao, G.; Yang, H.; Zhou, X.; Wu, Y. Dynamic control of double plasmon-induced transparencies in aperture-coupled waveguide-cavity system. *Plasmonics* **2018**, *13*, 345–352. [[CrossRef](#)]
10. Choi, S.; Jhang, K.Y. Thermal damages on the surface of a silicon wafer induced by a near-infrared laser. *Opt. Eng.* **2014**, *53*, 017103. [[CrossRef](#)]
11. Wu, X.; Zheng, Y.; Luo, Y.; Zhang, J.; Yi, Z.; Wu, X.; Wu, P. A four-band and polarization-independent BDS-based tunable absorber with high refractive index sensitivity. *Phys. Chem. Chem. Phys.* **2021**, *23*, 26864–26873. [[CrossRef](#)] [[PubMed](#)]

12. Neauport, J.; Lamaignere, L.; Bercegol, H.; Pilon, F.; Birolleau, J.C. Polishing-induced contamination of fused silica optics and laser induced damage density at 351 nm. *Opt. Express* **2005**, *13*, 10163–10171. [[CrossRef](#)] [[PubMed](#)]
13. Rämmer, A.; Osmani, O.; Rethfeld, B. Laser damage in silicon: Energy absorption, relaxation, and transport. *J. Appl. Phys.* **2014**, *116*, 053508. [[CrossRef](#)]
14. Bude, J.; Miller, P.E.; Shen, N.; Suratwala, T.; Laurence, T.; Steele, W.; Guss, G. Silica laser damage mechanisms, precursors, and their mitigation. In Proceedings of the Laser-Induced Damage in Optical Materials: 2014, Boulder, CO, USA, 14–17 September 2014; Volume 237, p. 92370S. [[CrossRef](#)]
15. Carr, C.W.; Bude, J.D.; DeMange, P. Laser-supported solid-state absorption fronts in silica. *Phys. Rev. B* **2010**, *82*, 184304. [[CrossRef](#)]
16. Zeng, Y.; Fan, X.; Chen, J.; He, S.; Yi, Z.; Ye, X.; Yi, Y. Preparation of composite micro/nano structure on the silicon surface by reactive ion etching: Enhanced anti-reflective and hydrophobic properties. *Superlattice Microst.* **2018**, *117*, 144–154. [[CrossRef](#)]
17. Fersman, I.A.; Khazov, L.D. The effect of surface cleanliness of optical elements on their radiation resistance. *Sov. J. Opt. Technol.* **1971**, *37*, 627–629.
18. Glebov, L.B. Intrinsic laser-induced breakdown of silicate glasses. In Proceedings of the Laser-Induced Damage in Optical Materials: 2001 International Society for Optics and Photonics, Boulder, CO, USA, 1–3 October 2001; Volume 4679, pp. 321–331. [[CrossRef](#)]
19. Zhang, W.; Shi, F.; Song, C.; Tian, Y.; Shen, Y. Study on the Absorption Characteristics and Laser Damage Properties of Fused Silica Optics under Flexible Polishing and Shallow DCE Process. *Micromachines* **2021**, *12*, 1226. [[CrossRef](#)]
20. Shao, T.; Shi, Z.; Sun, L.; Ye, X.; Huang, J.; Li, B.; Zheng, W. Role of each step in the combined treatment of reactive ion etching and dynamic chemical etching for improving the laser-induced damage resistance of fused silica. *Opt. Express* **2021**, *29*, 12365–12380. [[CrossRef](#)]
21. Adak, B.; Nash, P.; Chen, D.; Swiglo, A. Microstructural characterization of laser cladding of Cu-30Ni. *J. Mater. Sci.* **2005**, *40*, 2051–2054. [[CrossRef](#)]
22. Niederhauser, S.; Karlsson, B. Mechanical properties of laser clad steel. *Mater. Sci. Technol.* **2003**, *19*, 1611–1616. [[CrossRef](#)]
23. Huang, Y.L.; Liang, G.Y.; Su, J.Y.; Li, J.G. Interaction between laser beam and powder stream in the process of laser cladding with powder feeding. *Model. Simul. Mat. Sci. Eng.* **2004**, *13*, 47. [[CrossRef](#)]
24. Xie, X.; Peng, Q.; Chen, G.; Li, J.; Long, J.; Pan, G. Femtosecond laser modification of silicon carbide substrates and its influence on CMP process. *Ceram. Int.* **2021**, *47*, 13322–13330. [[CrossRef](#)]
25. Gao, B.; Guo, D.; Zhang, X.; Chen, G.; Pan, G. Picosecond Laser-Assisted Chemical Mechanical Polishing (CMP): Aiming at the Si-Face of Single-Crystal 6H-SiC Wafer. *ECS J. Solid State Sci. Technol.* **2021**, *10*, 044008. [[CrossRef](#)]
26. Shi, F.; Shu, Y.; Dai, Y.; Peng, X.; Li, S. Magnetorheological elastic super-smooth finishing for high-efficiency manufacturing of ultraviolet laser resistant optics. *Opt. Eng.* **2013**, *52*, 075104. [[CrossRef](#)]
27. Zhong, Y.; Dai, Y.; Shi, F.; Song, C.; Tian, Y.; Lin, Z.; Shen, Y. Effects of ion beam etching on the nanoscale damage precursor evolution of fused silica. *Materials* **2020**, *13*, 1294. [[CrossRef](#)]
28. Drescher, M.; Hentschel, M.; Kienberger, R.; Tempea, G.; Spielmann, C.; Reider, G.A.; Krausz, F. X-ray pulses approaching the attosecond frontier. *Science* **2001**, *291*, 1923–1927. [[CrossRef](#)]
29. Genin, F.Y.; Kozlowski, M.R.; Brusasco, R.M. Catastrophic failure of contaminated fused-silica optics at 355 nm. In Proceedings of the Solid State Lasers for Application to Inertial Confinement Fusion: Second Annual International Conference, Paris, France, 22–26 October 1996; Volume 3047, pp. 978–986.
30. Campbell, J.H.; Hawley-Fedder, R.A.; Stolz, C.J.; Menapace, J.A.; Borden, M.R.; Whitman, P.K.; Hackel, R.P. NIF optical materials and fabrication technologies: An overview. In Proceedings of the Optical Engineering at the Lawrence Livermore National Laboratory II: The National Ignition Facility, San Jose, CA, USA, 25–29 January 2004; Volume 5341, pp. 84–101. [[CrossRef](#)]
31. Demos, S.G.; Staggs, M. Application of fluorescence microscopy for noninvasive detection of surface contamination and precursors to laser-induced damage. *Appl. Opt.* **2002**, *41*, 1977–1983. [[CrossRef](#)]
32. Huang, J.; Wang, F.; Liu, H.; Geng, F.; Jiang, X.; Sun, L.; Sun, D. Non-destructive evaluation of UV pulse laser-induced damage performance of fused silica optics. *Sci. Rep.* **2017**, *7*, 1–12. [[CrossRef](#)]
33. Madison, K.W.; Patel, P.K.; Allen, M.; Price, D.; Fitzpatrick, R.; Ditmire, T. Role of laser-pulse duration in the neutron yield of deuterium cluster targets. *Phys. Rev. A* **2004**, *70*, 053201. [[CrossRef](#)]
34. Mutilba, U.; Gomez-Acedo, E.; Kortaberria, G.; Olarra, A.; Yagüe-Fabra, J.A. Traceability of on-machine tool measurement: Uncertainty budget assessment on shop floor conditions. *Measurement* **2019**, *135*, 180–188. [[CrossRef](#)]
35. Bonse, J.; Baudach, S.; Krüger, J.; Kautek, W.; Lenzner, M. Femtosecond laser ablation of silicon—modification thresholds and morphology. *Appl. Phys. A* **2002**, *74*, 19–25. [[CrossRef](#)]